JTTEE5 22:1184–1192
DOI: 10.1007/s11666-013-9978-8
1059-9630/$19.00 © ASM International

HVOF Coating Case Study for Power Plant Process Control Ball Valve Application

Luc Vernhes, David A. Lee, Dominique Poirier, Duanjie Li, and Jolanta E. Klemberg-Sapieha

(Submitted February 12, 2013; in revised form July 23, 2013)

This case study is the result of an investigation on HVOF 80/20 Cr_3C_2-NiCr coating failure of on-off metal-seated ball valve (MSBV) used in supercritical steam lines in a power plant and solution. HVOF 80/20 Cr_3C_2-NiCr coating is used to protect thousands of MSBVs without incident. However, in this case, the valves are challenged with exposure to rapid high-pressure and -temperature variations resulting in a unique situation where the coating experiences cracking and cohesive failure. It was found that carbide precipitation is a major factor causing embrittlement of the coating. Once the coating toughness and ductility is reduced, thermal, mechanical, and residual stresses can initiate and propagate cracks more easily, causing coating failure when exposed to thermal shock. To alleviate the above mentioned issues, possible coating alternatives were then evaluated.

Keywords chromium carbide, decarburization, failure mechanism, high temperature application, power plant, self-fluxing alloys

1. Introduction

Valves are being used on drain and vent lines to extract large quantity of condensate during power station start-up to get dry superheated steam rapidly. During normal operation, drain and vent valves must remain steam-tight to prevent energy loss and maximize plant efficiency. Over the last decade, metal-seated ball valves (MSBVs) have been the industry standard for this application, providing maintenance-free, tight, reliable shut-off. MSBVs considered in this study are of a floating ball design with a fixed seat. Ball and seat are manufactured from forged Inconel® 718 PH and coated with a HVOF 80/20 Cr_3C_2-NiCr coating. The primary function of the HVOF coating is to increase the load carrying capacity of the Inconel 718 surface*. Indeed, it has been demonstrated that the deposition of such thick coating will not only reduce the wear rate but also distribute the peak stresses generated by localized loading from the surface to the base material and increase the galling threshold resistance (resistance to adhesive wear and material transfer) (Ref 1, 2). 80/20 Cr_3C_2-NiCr coating composition is also specially adapted to offer resistance to the high-temperature, oxidizing conditions experienced by the valve (Ref 3, 4).

A major US-based power company had new challenges with their supercritical steam drain and vent lines in one of their plants. This particular fossil-fuel power station runs continuously from May to October because of high power demand to run air-conditioning systems. For the balance of the year, the plant only runs when the demand called for more power during peak usage times. Consequently, the operation of the plant changed from base-load to peaking. Every time the plant shuts down or start-up, MSBVs are frequently operated and exposed to supercritical steam, going up to 15 MPa (2200 psi) and 675 °C (1250°F) (Ref 5).

HVOF 80/20 Cr_3C_2-NiCr coating has failed after 1 year and less than 500 mechanical cycles in service on balls exposed to supercritical steam, with deterioration extending to regions where there is no contact between ball and seats. Coating was applied with a Diamond Jet® HVOF system using propylene as fuel. Visual examination of damaged components revealed minor frictional wear and typical stress/fatigue pattern (Fig. 1).

The intent of this failure analysis is first to provide valuable information to understand failure mechanism and to help in preventing this type of failure. The second objective of this study is to evaluate alternative coatings to alleviate those issues.

Section 2 describes the failure analysis, including experimental techniques, results, and discussion. Section 3 presents test results of potential solutions. Section 4 concludes.

Originally presented at the 2012 International Thermal Spray Conference and expanded from the original presentation. Thermal Spray 2012: Proceedings of the International Thermal Spray Conference, Air, Land, Water, and the Human Body: Thermal Spray Science and Applications, Houston, Texas, USA, May 21-24, 2012.

Luc Vernhes, Velan, Montreal, QC Canada; **David A. Lee**, Kennametal Stellite™, Goshen IN; **Dominique Poirier**, National Research Council of Canada, Boucherville, QC Canada; and **Duanjie Li** and **Jolanta E. Klemberg-Sapieha**, Department of Engineering Physics, Polytechnique Montreal, Montreal, QC Canada. Contact e-mail: luc.vernhes@velan.com.

*In this article, load carrying capacity refers to localized load as discussed by Holmberg et al. (Ref 2). This has to be distinguished from the structural load carrying capacity.

Fig. 1 HVOF 80/20 Cr_3C_2-NiCr coating exhibiting cohesive failure after 1 year in service

2. Failure Analysis

The failure analysis was conducted by elimination. A list of potential failure mechanisms was established based on the literature review and experience. Each potential failure mechanisms was investigated and eliminated if it was found not applicable:

(1) Coating quality:

- High porosity level, allowing high-pressure steam penetration;
- Lack of bonding between coating and substrate;
- Lack of bonding between splats;
- Embedded grit; and
- Residual stress (increase with thickness).

(2) Design:

- Mechanical stresses during operation (excessive load); and
- Thermal stresses due to thermal cycles or thermal shock.

(3) Phase changes:

- Corrosion;
- Reaction at interface;
- Oxidation; and
- Carbide precipitation.

The failure mechanisms have been attributed to either poor coating quality, improper ball valve design, or coating phase changes. Regarding coating quality, grit embedded at the interface is known to substantially lower coating adhesion. Embedded grit can also result in corrosion problems (Ref 6). Lack of bonding between coating and substrate results in a poor coating adhesion that can lead to premature coating spalling. Lack of bonding between splats results in a poor coating cohesive strength. Poor cohesion can lead to premature coating cracking and delamination (Ref 6). The structure of thermal-sprayed coatings, made of the piling up of splats, can produce significant interlamellar porosity. This porosity is usually associated with poorly melted particles that are trapped in the coatings. Porosity will not only decrease coating cohesive strength but can, if interconnected, act as a pathway enabling corroding or oxidizing elements to penetrate within the coating, and eventually reach the base material (Ref 6). Residual stresses are composed of quenching, cooling and peening stresses. They can limit coating adhesion and cohesion (Ref 6).

Failure mechanisms related to ball valve design were identified as mechanical stresses during operation (excessive load applied on the ball valve) or thermal stresses due to thermal cycles or thermal shock. Thermal stresses are caused by restricting thermal expansion. They are primarily a function of the coefficient of thermal expansion (CTE) mismatch, the variation in temperature (ΔT), and the Young modulus of the coating (E_c). The following equation is often used to get an approximation of the thermal stresses generated in a coating upon change in temperature (Ref 7, 8):

$$\sigma_{th} = E_c \Delta T (CTE_c - CTE_s) \quad \text{(Eq 1)}$$

It was also proposed that a chemical reaction at the coating/substrate interface could occur upon heating of the system. The species generated during such chemical reaction could be highly detrimental to coating performance and even lead to spallation. Oxidation of the Cr present in 80/20 Cr_3C_2-NiCr coatings at high temperature is well documented as a coating degradation mechanism (Ref 9). Carbide precipitation can occur because of the metastable nature of the thermal-sprayed 80/20 Cr_3C_2-NiCr coatings. During spraying, carbon is dissolved into the matrix. Carbon could come from two sources: (I) chrome carbides are getting partially dissolved, creating a range of Cr composition in matrix from carbon-rich to the original Ni alloy (the higher the spraying temperature, the more the dissolution that occurs); and (II) carbon comes also from the carbon-rich propylene fuel. The high cooling rate ''freezes'' the carbon-rich matrix in a supersaturated state, with amorphous or nanocrystalline zones—a metastable system that can change if heated (Ref 10).

A series of experiments were performed to find the most dominant failure mechanism.

2.1 Experimental Methodology

2.1.1 Coating Quality Characterization. SEM observation was used to compare a set of failed and new ball/seat. The interface between coating/substrate was qualitatively inspected by SEM observation. Coating thicknesses, porosity, and oxidation levels were measured. Coating microstructures were observed using field emission SEM (S4700, Hitachi Instruments Inc., Tokyo,

Table 1 Comparison of failed vs. new HVOF 80/20 Cr_3C_2 + [80Ni-20Cr] coating and OEM specification

	Failed component	New component	OEM specification
Thickness, μm	215	155 ± 35	200
Porosity, %	2	2	<3
Oxide, %	<2	<2	N/A
Bond, MPa	No failure	>70	>70
Microhardness (Vickers tip, 300 gf)	1092 ± 44	897 ± 69	>700

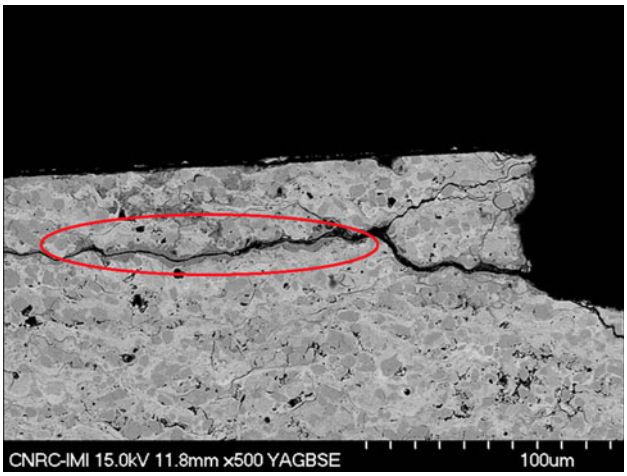

Fig. 2 HVOF 80/20 Cr_3C_2-NiCr coating, sprayed with C_3H_6 after 1 year in the field

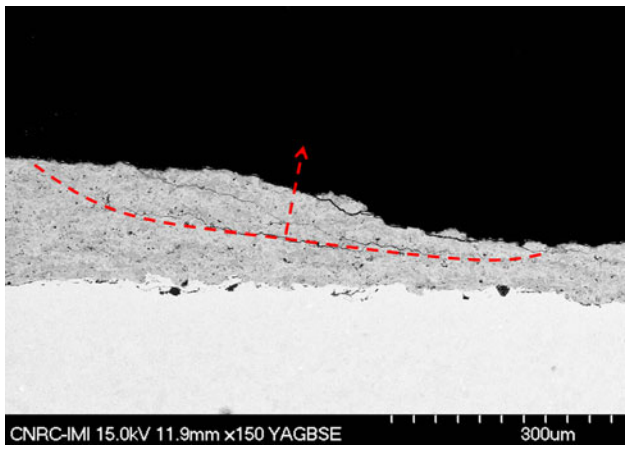

Fig. 3 HVOF 80/20 Cr_3C_2-NiCr coating, sprayed with C_3H_6 after 1 year in the field

Japan), while porosity levels were evaluated from image analysis on ten images obtained with the backscattered mode of an SEM equipment (JSM-6100, JEOL, Tokyo, Japan). Coating hardness values were measured using a Vickers microhardness tester (Micromet II, Buehler, Lake Bluff, IL, USA) operating under a 300 gf load. Nanohardness of coatings and of selected phases were evaluated using the Nano G200 from MTS/Nano Instruments (Oak Ridge, USA) with a Berkovitch tip under a load of 0.5 gf. The average micro and nanohardness values were obtained from ten and twenty indentations, respectively, performed on the cross sections of the coatings. Objective lenses were used with the nanoindenter when targeting specific phases. Otherwise, nanoindentations were performed randomly to get the overall coating nanohardness (average of all phases).

2.1.2 Valve Design. The second step was to perform two validation tests to confirm that valve design and materials were able to sustain localized load, wear, and thermal shock. For the load carrying capacity of the surface and wear-resistance test, one prototype valve was assembled with brand new coated components and connected to a 100 kW electrical boiler supplying superheated steam at 426 °C (800°F) and 12.5 MPa (1821 psig). The prototype valve was mechanically cycled using an automated pneumatic actuator, while monitoring seat leakage (in closed position). Valve was cycled every 2 min (open-to-close and close-to-open) under the steam atmosphere.

For the thermal shock test, new coated balls were heated to 675 °C (1247°F) for 30 min using a conventional electrical furnace. Balls were then quenched into room temperature water (20 °C-68°F).

2.1.3 Phase Changes. XRD measurements were performed on powder, and on ''as-sprayed'' and ''aged'' coatings to estimate changes in phase compositions and amorphous content as well as to determine the relative Crystallinity index (I_c) (Ref 11). I_c provides relative proportions of crystalline and amorphous phases. XRD measurements were performed between 30° and 55° temperature range because peaks and amorphous humps are found within those values for Cr_3C_2-based coatings. Crystallinity index is estimated based on the following formula:

$$I_c = \frac{\text{Sum of peak net areas}}{\text{Total net area}} \times 100 \qquad \text{(Eq 2)}$$

Measurements were performed using a D8 Advance Bruker AXS diffractometer (CuK_α, 40 mA and 40 kV). Spectrum areas were measured by means of Eva software.

2.1.4 Aging Test. As carbide reprecipitation (aging) process was suspected to take place on components exposed to temperature during service, an aging test was performed on the as-sprayed coating coupons at a higher temperature to exacerbate the phenomena and to grow visible carbides. Several HVOF-coated coupons were heated and maintained at 704 °C (1300°F) using an electrical furnace. Samples were then removed from the furnace at different intervals (4, 120, and 5040 h) and evaluated using SEM and XRD.

2.2 Results

2.2.1 Coating Quality Characterization. SEM observations and hardness measurements on failed and new coatings were compared with the original equipment manufacturer's (OEM) purchasing specification (see Table 1). One of the observations of the failed coating was the significant increase in microhardness values from nominal 900 HV (300 gf) up to 1400 HV (300 gf). This led to evaluation of the phase changes that were thought responsible for coating microhardness increase (Ref 12, 13).

Grit used to roughen the surface before coating was observed at the coating interface with the substrate, but was not excessive, and the spallation of the coating was not contributed by this contamination as coating had remained bonded. The coating that had spalled had delaminated above the bond line within the coating. Cracks observed in the remaining coating did not appear to originate at the coating/substrate interface or because of excess porosity. SEM also shows the presence of oxides (appearance in dark gray on backscattered electron images—see Fig. 2).

Cracks formed and propagated across the coating matrix or at the carbide/matrix interface, delaminating layer by layer the coating (see Fig. 3). Nanoindentation was used to measure the nanohardness of the oxide phase compared with the Cr_3C_2 phase and the overall coating nanohardness (see Table 2). Only an approximate value was determined for Cr_3C_2 because of the difficulty to target this specific phase during indentation. Among the different measurements, it appears that the oxide phase present in the coating shows the lowest hardness.

2.2.2 Valve Design. The prototype valve was able to perform over 2000 mechanical cycles with zero seat leakages. After disassembly and visual inspection, neither indentation nor excessive wear were observed on ball and seat surfaces confirming the load carrying capacity of the surface and the acceptable wear resistance of the coating, respectively.

On the other hand, after 30 consecutive thermal shocks going from 675 °C to ambient temperatures, HVOF 80/20 Cr_3C_2-NiCr exhibited a crack network highlighting that the thermal shock resistance of the coated ball was not adequate (see Fig. 4).

2.2.3 Phase Changes. Table 3 summarizes results and Fig. 5 shows both XRD spectra. The crystallinity index decreased by more than 35% after coating deposition, indicating the formation of amorphous phase and significant crystalline phase dissolution during spraying.

2.2.4 Aging Test. As shown on Fig. 6, carbide precipitation was observed under SEM after 4-h exposure to 704 °C (1300°F). Coarsening of the carbide precipitates together with growth of the initial carbides occurs after 120-h aging. XRD measurements were also performed on aged samples to estimate crystalline phase evolution during aging (see Fig. 7). Table 3 summarizes results. Carbide precipitation and growth were detected using the XRD method. The coating crystallinity indices increase after 4 h at 704 °C, reaching levels close to the initial powders (XRD peak sharpening due to recrystallization and carbide precipitation). The indices form plateau for longer aging time.

Table 2 Nanohardness of the oxide phase compared with the Cr_3C_2 phase and the overall coating nanohardness

	Nanohardness, GPa
New ball	15 ± 5
Damaged ball	18 ± 7
$H_{Cr_2O_3}$—Damaged ball	12 ± 1
$H_{Cr_3C_2}$—Damaged ball	~20

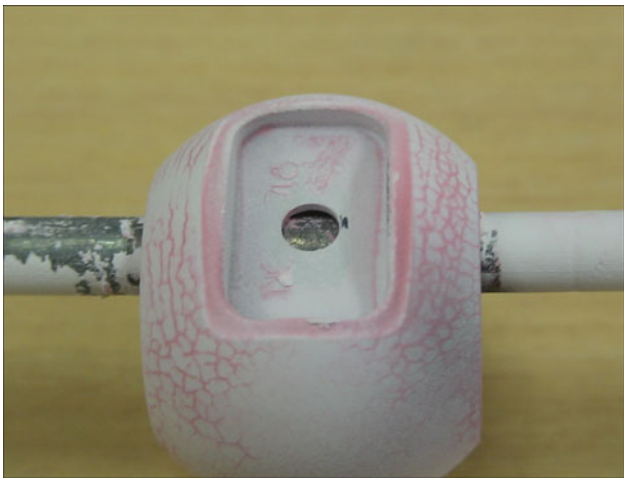

Fig. 4 HVOF 80/20 Cr_3C_2-NiCr coating, sprayed with C_3H_6, after 30 thermal shocks going from ambient temperatures to 675 °C

2.3 Discussion

The main difference observed between the failed versus the new ''as-sprayed'' coating is an increase in hardness by 25%, leading to measurements up to 1400 HV and

Table 3 Crystallinity indices of powder, "as-sprayed" and aged coating of the original HVOF coating

Powder composition	Fuel	Step	Crystallinity index, %
80% Cr_3C_2-20% [80Ni20Cr]	C_3H_6	Powder	77
		As sprayed	49
		4 h	67
		120 h	63
		5040 h	71

a decrease in thermal shock resistance. It was proposed that either carbide precipitation and/or oxidation could theoretically increase the hardness of the coatings and reduce its thermal shock resistance (aging). Thermal shock test results indicate that the CTE mismatch between HVOF 80/20 Cr_3C_2-NiCr (~$10 \times 10 \times 10^{-6}$/°C) and the Inconel 718 base material (~15.5×10^{-6}/°C) leads to high thermal stresses (Ref 7). After aging, thermal stresses generate crack leading to coating failure.

Therefore, the following two-step failure mechanism is suspected:

(1) *Carbon dissolution into 80% Ni-20% Cr binder during spraying*. Carbide dissolution occurring during spraying has a significant influence on the properties of 80/20 Cr_3C_2-NiCr coatings. For instance, plasma-sprayed coatings typically present extensive carbide dissolution and formation of brittle carbides and oxy-carbides over HVOF or detonation gun spray processes because of the higher particle in-flight temperature and residence time (Ref 14). This together with the higher porosity levels result in coatings with lower hardness displaying poorer performance in impact (Ref 15) and abrasion wear (Ref 16). The nature of the feedstock powder will also affect carbide degradation, and thus, performance of the coating (Ref 9). Carbide dissolution has a key role in changing the binder hardness as well as the phases present. It also appears that the resulting supersaturation of the NiCr matrix makes this phase prone to brittle cracking.

2(a) *Chrome carbide precipitation*. In high temperature service, matrix recrystallization can occur. The nucleation and growth of the carbide precipitates will depend not only on the heat-treatment temperature and time but also on the spraying parameters. For instance, an extensive dissolution during spraying will favor precipitation in the form of agglomeration of nucleated carbides, while with minimal dissolution, some growth around the retained carbides will preferentially occur (Ref 13). While those microstructural changes would happen in service for the 80/20 Cr_3C_2-NiCr coatings intended for high temperature applications, most of the studies replicate this condition by heat treating the coatings before testing. It has been shown that carbide precipitation can improve

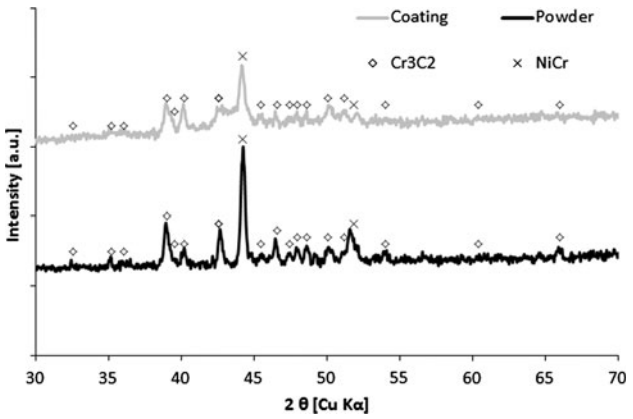

Fig. 5 XRD spectra of HVOF 80/20 Cr_3C_2-NiCr powder and coating, sprayed with C_3H_6. Cr_7C_3 and $Cr_{23}C_6$ phases, even though not shown on the graph, could also be present. Peaks overlapping has impeded their identification on all XRD spectra presented in this article

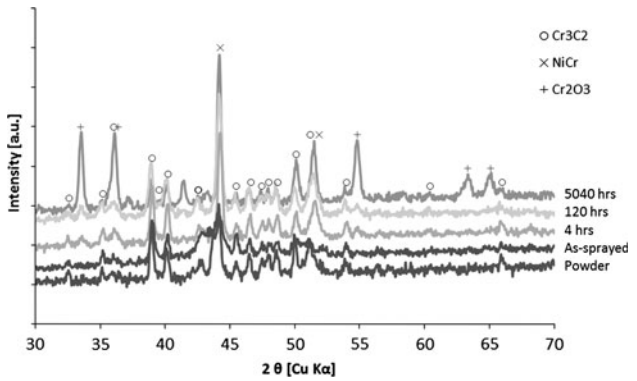

Fig. 7 XRD spectra of HVOF 80/20 Cr_3C_2-NiCr powder, ''as-sprayed'' and aged coatings, after 4- and 120-h exposure to 704 °C (1300°F), respectively

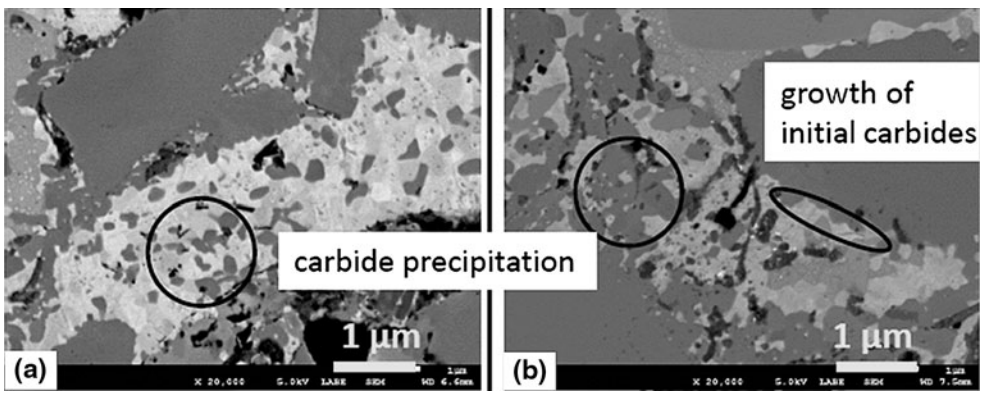

Fig. 6 Microstructural evolution during aging test at 704 °C (1300°F) after (a) 4-h exposure; (b) 120-h exposure

coating's wear resistance, adhesion, and hardness (Ref 13, 17, 18). Hardness increase could be observed with values exceeding the coating initial hardness because of carbide precipitation and to a "sintering" effect (decrease in porosity and improved adhesion between splats). The hardness increase could keep increasing because of the formation of a fine carbide network (Ref 13, 19).

2(b) *Chrome oxidation*. When sufficient Cr_3C_2 dissolution occurs during spraying to get at least 27.5% Cr in the matrix (either due to spraying conditions or the type of powder used), only Cr_2O_3 is formed in a continuous layer (Ref 17). Cr_3O_2 can be adherent to the surface or eventually buckled if carbides are large. If there is not enough Cr in solution in the matrix, then a NiO scale forms below which a continuous Cr_2O_3 scale develops. NiO can further be consumed to form $NiCr_2O_4$ (Ref 20).

Water vapor-containing atmospheres cause more rapid oxidation of chromia-forming alloys than do dry oxygen or air, according to the equation shown below (Ref 21):

$$\frac{1}{2}Cr_2O_3\ (s) + H_2O\ (g) + \frac{3}{4}O_2\ (g) = CrO_2(OH)_2\ (g) \quad \text{(Eq 3)}$$

In summary, two reactions involving Cr are competing: Cr can form carbides or can oxidize. At the temperatures of interest in this study, i.e., 675 °C or lower, Cr and C diffusions are slow, and it is most probable that the Cr in contact with the oxidizing atmosphere will preferentially form oxides (Ref 17) . However, the Cr present deeper in the coating and not in contact with O_2 would form carbides.

In this specific case, regions of oxides displaying low hardness have been observed (Table 2), possibly because of the presence of pores and cracks, and perhaps the formation of nonstable oxides. Furthermore, no significant

Fig. 8 Coating #1, #2, and #3 were repeatedly subjected to thermal shocks going from ambient temperatures to 675 °C. Then they were put through liquid penetrant tests to check for any cracking

Table 4 List of potential solutions

#	Chemical composition: Powder	Fuel	Process	Nominal thickness, µm	Remark
0	80% $Cr_3C_2$20% [80Ni20Cr]	C_3H_6	HVOF	200	Original (failed)
1	75% $Cr_3C_2$25% [80Ni20Cr]	H_2		200	25% matrix to increase ductility
2	65-70% WC22-25% $Cr_3C_2$7% [Ni/NiCr]	H_2		200	Almost chrome-free binder to minimize Cr_3C_2 and Cr_3O_2 formation
3	55% Ni, 17% W, 15% Cr,4% Si3.5% Fe3% B <1% C	H_2	Spray and Fuse	300	55% Ni to provide ductility. Fusing at 1000 °C to sinter, stress relieve and precipitate carbon.

trend in change of hardness from coating top to bottom, where a gradient in oxide concentration is expected, was observed. With Cr_2O_3 hardness being around 12 GPa and Cr_3C_2 hardness around 20 GPa, the precipitation of extra carbides seems a reasonable explanation for the increase in overall coating hardness.

No fine chrome carbides have been detected under SEM into the NiCr binder presumably because of very small-sized crystals.

3. Solution

The next step was to test and qualify potential coating solutions, better suited to carry high load at elevated temperature and to withstand thermal shock.

Based on our analysis, the dominant failure mechanism is coating embrittlement due to chrome carbide precipitation in-service across coating binder which reduces coating thermal shock resistance. Three potential coating formulations were selected to overcome this issue.

The first candidate, coating #1, was a 75/25 Cr_3C_2-NiCr coating having a higher binder/carbide ratio compared with the standard to provide a slightly softer but tougher coating (Ref 7). The second candidate, coating #2, was a coating with a chrome-free binder to minimize the risk of carbide precipitation. To compensate for hardness reduction due to the lack of chromium, tungsten carbides were added to the chrome carbides. The third solution, coating #3, was a Ni-based fused and sintered coating having chemical composition closer to the base material and being fused at 1000 °C to sinter, stress relieve, and precipitate carbon. The CTE of Ni-based fused and sintered coating (~16×10^{-6}/°C versus ~10×10^{-6}/°C for 80/20 Cr_3C_2-NiCr coatings) more closely matches that of Inconel (~15.5×10^{-6}/°C) (Ref 22). Consequently, the Ni-based fused and sintered coating induces less thermal stresses because of CTE mismatch than HVOF 80/20 Cr_3C_2-NiCr when applied on Inconel.

To minimize carbon dissolution during spraying, hydrogen was used instead of propylene (carbon-free fuel) and Jet-Kote® HVOF system was used instead of Diamond Jet® (lower in-flight temperature). Table 4 summarizes the selected potential solutions.

Brand new samples were produced with those three new coatings. A battery of tests was performed to assess their behavior for this specific application.

Table 5 Crystallinity indices of powder and "as-sprayed" HVOF coating

	Crystallinity index	
Coating ID	**Powder, %**	**Coating, %**
0	77	49
1	80	51
2	83	82

3.1 Valve Design

Load carrying capacities of the surface and wear resistances of the three coatings were evaluated using the cycle test as previously described. Coatings #1 and #3 exhibited similar mechanical resistances than the original HVOF coating, as expected, based on the literature review (Ref 23). Coating #2 demonstrated exceptionally superior mechanical resistance by performing five times more mechanical cycles than the original coating without any leakage. The excellent wear behavior of HVOF (W,Cr)C-Ni in dry sliding condition is attributable to the presence of two hard phases : WC and $(W,Cr)_2C$. As studied by Berger et al. (Ref 24), such a material combination results in a hardness value of over 1200 HV (300 gf) providing superior tribological performance at high temperature (Ref 25, 26).

Thermal stress resistance was evaluated using the thermal shock test previously described. Coating #1 exhibited a crack network relatively similar to the one observed on the failed valves after 60 thermal shock cycles. Coating #2 exhibited cracking and delamination after exposure to 675 °C for 30 min. As described by Hou et al. (Ref 27), HVOF (W,Cr)C-Ni coating is able to well retain hard WC phase at temperatures higher than WC but not as high as 80/20 Cr_3C_2-NiCr coatings and exhibits excellent oxidation resistance. However, the relatively low CTE of WC compared with nickel-iron-based superalloys substrate engenders high interfacial stresses at elevated temperature leading to delamination and crack formation as documented by Miller and Lowell (Ref 28) when on the other hand, the CTE of Cr_3C_2 is close to the one of nickel and iron (Ref 29). Coating #3 successfully passed the thermal shock test (No crack indication after 60 thermal cycles—see Fig. 8).

3.2 Phase Changes

The third test was to perform XRD measurements on powder and "as sprayed" for the HVOF coatings to estimate crystalline phases dissolution during deposition. The fusing process allowing stress relieving and carbon

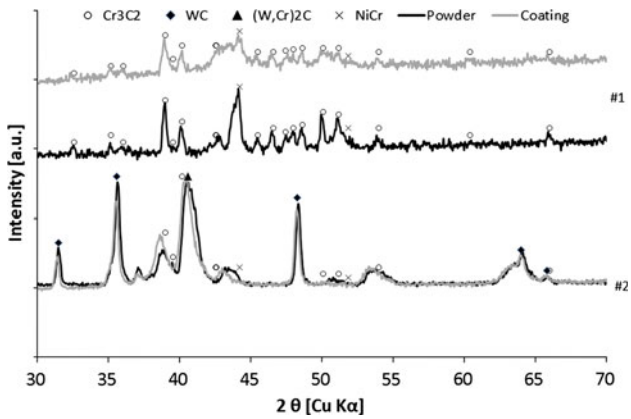

Fig. 9 XRD spectra of HVOF material #1 and #2; powder and "as-sprayed" coating

precipitation, the I_c of coating #3 was not evaluated. Table 5 summarizes results.

While coating #1 displays similar degradation level to the original coating, coating #2 crystallinity index remains much higher, indicating less amorphization (see Fig. 9). However, for coating #2, a partial phase transformation ($WC \rightarrow W_2C$) was observed on the XRD spectra after deposition. Therefore, amorphization is not the only mechanism responsible for the degradation of the material with this composition.

Based on those data, coating #3 appears well suited to withstand high bearing load and thermal shock. The coating #3 seems also the least sensitive to aging at high temperatures and therefore more durable under these very specific conditions.

Coating #2 is not suitable for temperature over 540 °C (1000°F). However, it has demonstrated the best overall performance at lower temperatures.

4. Conclusion

In this study, the failure of a HVOF 80/20 Cr_3C_2-NiCr coating applied on a MSBV used in supercritical steam line was investigated. While oxidation definitely contributes to coating degradation, it is believed that carbide precipitation is the major factor causing embrittlement of the coating. Once the coating's toughness and ductility are reduced, thermal, mechanical, and residual stresses can initiate and propagate cracks more easily, causing coating failure when exposed to thermal shock.

A spray-and-fuse NiWCrBSi coating being more suitable to withstand high bearing load when facing thermal shock was qualified. This coating is less sensitive to aging at high temperatures and, therefore, more durable under these very specific conditions.

Using this technology, new valves were installed in the plant, and they have successfully been work for the last two years.

Acknowledgments

The authors wish to thank Mr. Subhash Saini (Velan), Michel Thibodeau (NRC), and Jimmy Sykes (NRC) for their technical support, as well as Dr. Rogerio Lima (NRC) for useful discussion. The authors also greatly appreciate Velan's interest in and support for this research.

References

1. G. Bolelli, L. Lusvarghi, M. Montecchi, P. Mantini, F. Pitacco, H. Volz, and M. Barletta, HVOF-Sprayed WC-Co as Hard Interlayer for DLC Films, *Surf. Coat. Technol.*, 2008, **203**(1), p 699-703
2. K. Holmberg, A. Laukkanen, H. Ronkainen, K. Wallin, and J.K. Simo Varjus, Tribological Contact Analysis of a rigid Ball Sliding on a Hard Coated Surface Part II: Material Deformations, Influence of Coating Thickness and Young Modulus, *Surf. Coat. Technol.*, 2006, **200**(1), p 3810-3823
3. K.N. Lee, D.S. Fox, J.I. Eldridge, Z. Dongming, R.C. Robinson, N.P. Bansal, and R.A. Miller, Upper Temperature Limit of Environmental Barrier Coatings Based on Mullite and BSAS, *J. Am. Ceram. Soc.*, 2003, **86**(8), p 1299-1306
4. C.P. Bergmann, J. Vicenzi, D.L. Villanova, M.D. Lima, A.S. Takimi, and C.M. Marques, HVOF-Coatings Against High Temperature Erosion (~300 C) by Coal Fly Ash in Thermoelectric Power Plant, *Mater. Des.*, 2006, **27**(3), p 236-242
5. D. Xu, J. Bao, and Y. Jin, Mechanical Jamming Analysis of the Reheat-Stop-Valve Mechanism in the Supercritical Steam Turbine, *J. Mech. Eng.*, 2010, **46**(1), p 121-127
6. J.R. Davis, *Handbook of Thermal Spray Technology*, ASM International, Materials Park, OH, 2000
7. M. Antonov and I. Hussainova, Thermophysical Properties and Thermal Shock Resistance of Chromium Carbide Based Cermets, *Proc. Estonian Acad. Sci.*, 2006, **12**(4), p 358-367
8. A. Tipton, *The Effect of HVOF Thermal Spray on the Elevated Temperature High Cycle Fatigue Behavior of a Martensitic Stainless Steel*, Dresser-Rand, New York, NY, 2002
9. S. Wirojanupatump, P.H. Shipway, and D.G. McCartney, The Influence of HVOF Powder Feedstock Characteristics on the Abrasive Wear Behaviour of CrxCy-NiCr Coatings, *Wear*, 2001, **249**(9), p 829-837
10. S. Matthews, M. Hyland, and B. James, Long-Term Carbide Development in High-Velocity Oxygen Fuel/High-Velocity Air Fuel Cr_3C_2-NiCr Coatings Heat Treated at 900 °C, *J. Therm. Spray Technol.*, 2004, **13**(4), p 526-536
11. C. Verdon, A. Karimi, and J.L. Martin, A Study of High Velocity Oxy-Fuel Thermally Sprayed Tungsten Carbide Based Coatings. Part 1. Microstructures, *Mater. Sci. Eng. A Struct. Mater. Prop. Microstruct. Process.*, 1998, **A246**(1-2), p 11-24
12. T.A. Taylor, Phase Stability of Chrome-Carbide Ni-Cr Coatings in Low-Oxygen Environments, *Proceedings of the 2nd Conference on Structure/Property Relationships in Thick Films and Bulk Coatings*, 10-12 Feb. 1975, 4th ed., 1975, p 790-794
13. S. Matthews, M. Hyland, and B. James, Microhardness Variation in Relation to Carbide Development in Heat Treated Cr_3C_2-NiCr Thermal Spray Coatings, *Acta Mater.*, 2003, **51**(14), p 4267-4277
14. V.N. Shukla, V.K. Tewari, and R. Jayaganthan, Comparison of Tribological Behavior of Cr_3C_2/NiCr Coatings Deposited by Different Thermal Spray Techniques: A Review, *Int. J. Mater. Sci. Eng.*, 2011, **2**(1), p 1-2
15. X.M. Li, Y.Y. Yang, T.M. Shao, Y.S. Jin, and G. Barbezat, Impact Wear Performances of Cr_3C_2-NiCr Coatings by Plasma and HVOF Spraying, *Wear*, 1997, **202**(2), p 208-214
16. G. Barbezat, A.R. Nicoll, and A. Sickinger, Abrasion, Erosion and Scuffing Resistance of Carbide and Oxide Ceramic Thermal Sprayed Coatings for Different Applications, *Wear*, 1993, **162-164**(pt A), p 529-537
17. S. Matthews, B. James, and M. Hyland, The Role of Microstructure in the High Temperature Oxidation Mechanism of Cr_3C_2-NiCr Composite Coatings, *Corros. Sci.*, 2009, **51**(5), p 1172-1180
18. J.M. Guilemany, J.M. Miguel, S. Vizcaino, C. Lorenzana, J. Delgado, and J. Sanchez, Role of Heat Treatments in the Improvement of the Sliding Wear Properties of Cr_3C_2-NiCr Coatings, *Surf. Coat. Technol.*, 2002, **157**(2-3), p 207-213
19. J.M. Guilemany, J. Nutting, and N. Llorca-Isern, Microstructural Examination of HVOF Chromium Carbide Coatings for High-Temperature Applications, *J. Therm. Spray Technol.*, 1996, **5**(4), p 483-489
20. S. Matthews, B. James, and M. Hyland, Erosion of Oxide Scales Formed on Cr_3C_2-NiCr Thermal Spray Coatings, *Corros. Sci.*, 2008, **50**(11), p 3087-3094
21. N.K. Othman, J. Zhang, and D.J. Young, Effect of Water Vapour on Cyclic Oxidation of Fe-Cr Alloys, *Mater. Corros.*, 2011, **62**(6), p 496-503
22. P. Berthod and L. Aranda, Thermal Expansion Behaviour of Ternary Nickel-Based, Cobalt-Based, and Iron-Based Alloys Containing Very High Fractions of Carbides, *ISRN Metall.*, 2012, **2012**(1), p 1-9
23. H.-J. Kim, S.-Y. Hwang, C.-H. Lee, and P. Juvanon, Assessment of Wear Performance of Flame Sprayed and Fused Ni-Based Coatings, *Surf. Coat. Technol.*, 2003, **172**(2-3), p 262-269

24. L.M. Berger, S. Saaro, T. Naumann, M. Kasparova, and F. Zahalka, Microstructure and Properties of HVOF-Sprayed WC-(W, Cr)2C-Ni Coatings, *J. Therm. Spray Technol.*, 2008, **17**(3), p 395-403
25. Y. Ishikawa, S. Kuroda, J. Kawakita, Y. Sakamoto, and M. Takaya, Sliding Wear Properties of HVOF Sprayed WC-20%Cr_3C_2-7%Ni Cermet Coatings, *Surf. Coat. Technol.*, 2007, **201**(8), p 4718-4727
26. L.M. Berger, S. Saaro, T. Naumann, M. Kašparova, and F. Zahálka, Influence of Feedstock Powder Characteristics and Spray Processes on Microstructure and Properties of WC-(W, Cr)2C-Ni Hardmetal Coatings, *Surf. Coat. Technol.*, 2010, **205**(4), p 1080-1087
27. G.-L. Hou, H.-D. Zhou, Y.-L. An, G. Liu, J.-M. Chen, and J. Chen, Microstructure and High-Temperature Friction and Wear Behavior of WC-(W, Cr)2C-Ni Coating Prepared by High Velocity Oxy-Fuel Spraying, *Surf. Coat. Technol.*, 2011, **206**(1), p 82-94
28. R.A. Miller and C.E. Lowell, Failure Mechanisms of Thermal Barrier Coatings Exposed to Elevated Temperatures, *Thin Solid Films*, 1982, **95**(3), p 265-273
29. M. Kaur, H. Singh, and S. Prakash, *High-Temperature Behavior of a High-Velocity Oxy-Fuel Sprayed Cr_3C_2-NiCr Coating*, 8th ed., Springer, Boston, 2012, p 2979-2993